Colloids and Surfaces B: Biointerfaces 243 (2024) 114154

Contents lists available at ScienceDirect

Colloids and Surfaces B: Biointerfaces

journal homepage: www.elsevier.com/locate/colsurfb

Mn^{2+} vs Co^{2+} substitution into β-TCP: Structural details and bone cells response

Elisa Boanini [a,*], Stefania Pagani [b], Massimo Gazzano [c], Katia Rubini [a], Lavinia Raimondi [d], Angela De Luca [d], Alessia Romanelli [b], Gianluca Giavaresi [b], Adriana Bigi [a]

[a] Department of Chemistry "Giacomo Ciamician", Alma Mater Studiorum - University of Bologna, Bologna 40126, Italy
[b] CS-Surgical Sciences and Technologies, IRCCS Istituto Ortopedico Rizzoli, Bologna 40136, Italy
[c] ISOF-CNR, Bologna 40129, Italy
[d] CS-Surgical Sciences and Technologies-SS Omics Science Platform for Personalized Orthopedics, IRCCS Istituto Ortopedico Rizzoli, Bologna 40136, Italy

ARTICLE INFO

Keywords:
Osteogenesis
Calcium phosphate
Angiogenesis
Osteoblast
Osteoclast

ABSTRACT

This work investigated the range of substitution of two biologically relevant ions, namely Mn^{2+} and Co^{2+}, into the structure of β-tricalcium phosphate, as well as their influence on bone cells response. To this aim, β-TCP was synthesized by solid state reaction in the presence of increasing amount of the substituent ions. The results of the X-ray diffraction analysis reveal that just limited amounts of these ions can enter into the β-TCP structure: 15 at% and 20 at% for cobalt and manganese, respectively. Substitution provokes aggregation of the micrometric particles and reduction of the lattice constants. In particular, the dimension of the *c*-parameter exhibits a discontinuity at about 10 at% for both cations, although with different trend. Moreover, Rietveld refinement demonstrates a clear preference of both manganese and cobalt for the octahedral site (V). The influence of these ions on cell response was tested on osteoblast, osteoclast and endothelial cells. The results indicate that the presence of manganese promotes a good osteoblast viability, significantly enhances the expression of osteoblast key genes and the angiogenic process of endothelial cells, while inhibiting osteoclast resorption. At variance, osteoblast viability appears reduced in the presence of Co samples, on which osteoblast genes reach higher expression than on β-TCP just in a few cases. On the other hand, the results clearly show that cobalt significantly stimulates the angiogenic process and inhibits osteoclast resorption.

1. Introduction

The possibility of calcium orthophosphates (CaPs) to support ionic substitution depends on several factors, such as the difference in the dimensions of ionic radii, charge and electronegativity, between the substituted and the substituent element. Moreover, an important role is played by the structure flexibility of the CaP [1,2], which can allow substitution in the whole range of composition, or just in a limited amount. X-ray diffraction analysis is the election technique to discriminate between simple ion doping and ionic substitution, which provokes structural modifications and influences the chemistry, the morphology and the biological properties of the host calcium phosphate [2–7]. CaPs are of great interest as components of biomaterials for the repair and substitution of damaged hard tissues, and ionic substitution can indeed improve their biological performance [8–14]. Among CaPs, β-tricalcium phosphate ($Ca_3(PO_4)_2$, β-TCP) is osteoconductive and osteoinductive, and the amount of its applications as bone graft is second only to those of hydroxyapatite (HA) [15]. The rhombohedral cell of β-TCP (space group *R3c*) contains 21 formula units. Ca atoms are distributed in five different sites: three Ca sites are on general positions with a multiplicity of 18 (Ca (I), Ca(II) and Ca(III)), whereas Ca(IV) and Ca(V) are on special positions with multiplicity reduced to 6. Furthermore, just half of the Ca(IV) sites are occupied [16–18]. Recent studies based on atomistic simulations revealed that β-TCP properties could depend on the possible ordering of Ca(IV) site occupancy [19]. Two of the three crystallographic independent phosphorus atoms, namely P(II) and P(III), are on general positions, whereas P(I) is on a special position. Several divalent cations can replace calcium in the structure of β-TCP [5,10,15,20]. Cations smaller than calcium, such as Mg^{2+} and Zn^{2+}, usually exhibit a structural preference for Ca(V); on the other hand, bigger cations, such as Sr^{2+}, prefer different sites and can reach much larger values of substitution [10,15, 18].

* Corresponding author.
E-mail address: elisa.boanini@unibo.it (E. Boanini).

https://doi.org/10.1016/j.colsurfb.2024.114154
Received 29 May 2024; Received in revised form 24 July 2024; Accepted 7 August 2024
Available online 8 August 2024

Herein, we report the results of a study on the incorporation of Co^{2+} and Mn^{2+} into the structure of β-TCP. Cobalt is an essential trace element, which plays a role as cofactor of many metalloproteins, and has been reported to promote angiogenesis and osteogenesis [21–24]. Manganese is an essential micronutrient involved in the formation of bone; it displays antioxidant properties and it acts as cofactor for several enzymes [10,25]. Moreover, both Co^{2+} and Mn^{2+} have been shown to play a beneficial role on bone cells when associated to CaPs [21, 25–32]. β-TCP doped with cobalt, as well as with manganese, was investigated by many Authors [10, 27, 32–37]. However, just a few studies discriminate between doping and ionic substitution on the basis of structural modifications [35–37]. Ionic substitution implies regular substitution of an ion of the host structure (Ca in the present case) with a different ion (Co or Mn). At variance, ion doping is not associated with a regular substitution, and the doping ion can be just adsorbed on the host structure [2].

No definitive data on the range of possible incorporation of these ions into the structure of β-TCP has been reported up to now, and the influence of the substitution on structural details has not been clarified. Again, most studies focus on materials prepared by precipitation followed by heat treatment and report just the amount of foreign ion in solution, but not in the solid phase.

In this work, we prepared Co and Mn substituted β-TCP through solid state reaction at high temperature [15,16,20] with the aim to investigate the range of possible substitution and the structural modifications induced by the incorporation of the foreign ions, as well as their influence on cell response.

As cobalt and manganese in doped β-TCP are known to positively influence the bone biology, as reported above, it is essential to evaluate how these innovative materials (Co and Mn substituted β-TCP) interact with osteoblasts, osteoclasts and endothelial cells. In this study we first focused on osteoblasts, seeded in direct contact with the materials and evaluated in term of viability and expression of their most important genes. Secondly, we wanted to observe how material-conditioned pre-osteoblasts changed the microenvironment and consequently influenced other cell types. For this reason, the supernatants of these cultures were also used to indirectly evaluate the role of Co and Mn substituted β-TCP on the osteoclast activity (by bone resorption pit assay) and endothelial cells (by tubule formation assay).

2. Materials and methods

2.1. Materials synthesis

Dicalcium phosphate dihydrate (DCPD, $CaHPO_4{\cdot}2\ H_2O$) was synthesized using 600 ml of a phosphate solution containing 0.08 mol of $Na_2HPO_4{\bullet}12\ H_2O$ and 0.08 mol of $NaH_2PO_4{\bullet}H_2O$, pH 4 adjusted with CH_3COOH. The solution was heated at 37 °C, afterwards 200 ml of solution containing 0.16 mol of $Ca(CH_3COO)_2H_2O$ was added drop-wise over a period of about 60 min, under stirring. the precipitate was stored in contact with the mother solution for 10 min, filtered, repeatedly washed with bidistilled water and dried at 37 °C.

β-TCP was obtained by solid state reaction of a mixture of $CaCO_3$ and freshly prepared DCPD that were carefully ground together in the molar ratio of 1:2, then kept at 1000°C for 10 h.

For the preparation of Mn-substituted β-TCP, α-$Mn_3(PO_4)_2$ was obtained by solid state reaction of a mixture of $MnCO_3$ and $NH_4H_2PO_4$ in the molar ratio of 3:2 at 1000 °C for 12 h. Mn-substituted β-TCP samples, with a Mn content 1 2, 5, 10, 20, 25 mol% (calculated on total cations Ca+Mn), were prepared by heat treatment of appropriate stoichiometric mixtures of β-TCP and α-$Mn_3(PO_4)_2$ at 1200° C for 12 h. Samples were labeled Mn1, Mn2, Mn5, Mn10, Mn20 and Mn25, respectively.

For the preparation of Co-substituted β-TCP, α-$Co_3(PO_4)_2$ was obtained by solid state reaction of a mixture of 2CoCO3•3Co(OH)2•10H2O and $NH_4H_2PO_4$ in the molar ratio of 3:10 at 1000°C for 12 h.

Co-substituted β-TCP samples, with a Co content 1, 2, 5, 10, 15, 20 mol% (calculated on total cations Ca+Co), were prepared by heat treatment of appropriate stoichiometric mixtures of β-TCP and α-$Co_3(PO_4)_2$ at 1200°C for 12 h. Samples were labeled Co1, Co2, Co5, Co10, Co15 and Co20, respectively.

For both Co- and Mn-substituted β-TCP, the temperature of 1200°C, higher than the α→β transition in pure β-TCP (1125 °C) was necessary due to the presence of the substituting ion [38].

2.2. Physico-chemical characterization of materials

X-ray diffraction (XRD) measurements were performed using an X'PertPro diffractometer (PANalytical, Almelo, The Netherlands) equipped with a solid-state X'Celerator detector and a copper X-ray source (X-ray wavelength = 0.15418 nm). Data scans were collected with divergence and anti-scatter slits of 1°, moving in 0.05° steps, at a rate of 40 s/step for qualitative measurements and with ½° slits, moving 0.0131° steps and collecting for 180 s/step for structural investigations.

In vitro tests were performed on disk-shaped samples (∅ = 6.0 mm). Each disk was prepared by pressing 40 mg of powder into cylindrical molds using a standard evacuable pellet die (Hellma Italia Srl, Milano, Italy) and sterilized using gamma rays (Cobalt-60) at a dose of 25 kGy.

Morphological investigation of the as-synthesized crystals and the disk-shaped samples surface was performed using a Zeiss Leo-1530 (Zeiss Microscopy, Milano, Italy) high resolution scanning electron microscope (SEM) operating at 5 kV (SE detector). The samples were sputter-coated with gold before observation.

Release of Mn or Co from disk-shaped samples in cell growth medium (detailed in *Cell cultures* paragraph) was measured up to 14 days by Agilent 4210 (Agilent, Santa Clara, CA, USA) Molecular Plasma-Atomic Emission Spectroscopy (MP-AES). Manganese line at 403.307 and cobalt line at 350.228 nm were used. The volume of the release solution utilized for each disk-shaped sample was 1 ml. Results from this analysis represent the mean value of three different determinations.

2.3. Biological tests

Biological tests were performed on Mn- and Co-substituted β-TCP disk-shaped samples with low amount of substitution: 1, 2 and 5 mol%.

2.3.1. Cell cultures

The biomaterials were tested with mouse calvarial preosteoblast MC3T3-E1 Subclone 4 cell line (American Type Culture Collection (ATCC) CRL-2593). Cells were cultured in αMEM, nucleosides, no ascorbic acid (GIBCO™, ThermoFisher Scientific, Waltham, MA, USA) supplemented with 10 % fetal bovine serum (FBS, Lonza, Verviers, Belgium), 100 U/ml penicillin and 100 μg/ml streptomycin (Gibco, Life Technologies, Carlsbad, CA) and expanded in standard conditions at 37 °C in a humidified 95 %air/5 %CO_2 atmosphere. Before cell seeding the materials were placed in 24-wells plates and preconditioned for two hours with growth medium. MC3T3 were then counted and seeded on the material upper surface at the density of 5×10^4 cells/cm^2 for 24 hrs, 2×10^4 cells/cm^2 for 7 and 14 days in differentiating medium: αMEM added with 50 μg/ml ascorbic acid and 10 mM β glycerophosphate (Sigma Aldrich, St. Louis, MO, USA). The same cell number was seeded directly on the bottom well to have an internal control of the cultures.

At each timepoint the supernatants were harvested in sterile conditions and centrifuged to eliminate residual powder released by the materials. These conditioned media were kept at −80 °C until the performing of the next assays.

2.3.2. Cell viability

Cell viability was quantified after 1, 7 and 14 days. Alamar Blue™ dye (Invitrogen, Life Technologies Corporation, EUGENE, OR, USA) was added 1:10 v/v in culture medium and incubated for 4 h at 37 °C. This non-toxic reagent allows us to evaluate the cell activity on the same culture at different endpoints by the chemical reduction of its main

oxidized blue compound (resazurin), which turns towards the purple color in the mitochondria of living cells. The fluorescent product was quantified by a Micro Plate reader (VICTOR X2030, Perkin Elmer, Milano, Italy) at 530 ex–590 em nm wavelengths and expressed as relative fluorescence units (RFU).

2.3.3. Gene expression analysis

Gene expression of the most common markers of osteoblast activity was evaluated after all culture timepoints by Real-Time semi-quantitative PCR. Total RNA was extracted using Trizol® reagent (AMBION by Life Technologies, Carlsbad, CA, USA) and Chloroform (Sigma Aldrich) until harvesting the aqueous phase. The procedure was completed using the commercial PureLinkTM RNeasy Mini Kit (AMBION). The obtained RNA was then quantified by a NanoDrop spectrophotometer (Thermo Fisher Scientific) and reverse transcribed with SuperScriptVILO cDNA Synthesis Kit (Life Technologies) following the manufacturer's instructions, in a Thermal Cycler (ThermoCycler 2720, Applied Biosystem by Life Technologies, Monza, Italy). The obtained cDNA of each sample was diluted to the final concentration of 5 ng/µl and 10 ng were tested in duplicate for each sample. Gene expression was evaluated with semi-quantitative Real-Time PCR analysis using a QuantiTect SYBR Green PCR Kit (Qiagen GmbH, Hilden, Germany) in a LightCycler 2.0 Instrument (Roche Diagnostics GmbH, Manheim, Germany). The protocol included a denaturation cycle at 95 °C for 15 min, 25–40 cycles of amplification (95 °C for 15 sec, an appropriate annealing temperature for each target for 20 sec, and 72°C for 20 sec), and a melting curve analysis to check for amplicon specificity. The primers used to evaluate gene expression are detailed in Table S1. The threshold cycle was determined for each sample and used to calculate relative expression by applying the Livak method ($2^{-\Delta\Delta Ct}$), with GAPDH as reference gene and TCP sample as calibrator [39].

2.3.4. Tubule formation assay

An *in vitro* tube formation assay was performed to observe the effect of Co (1,2,5), Mn (1,2,5), and β-TCP scaffolds on the angiogenic process of human umbilical vein endothelial cells (HUVEC; CRL-4053), which were purchased from ATCC and cultured in Vascular Cell Basal Medium (ATCC PCS-100–030) supplemented with Endothelial Cell Growth Kit (ATCC PCS-110–041), 100 U/ml penicillin and 100 µg/ml streptomycin. Briefly, a 96-well plate (Corning, Bedford, MA) was coated with Matrigel® matrix (Corning, Bedford, MA) and allowed to fully gel at 37 °C for 1 hr. HUVECs cells were seeded at a density of 30.000 cells/well on the Matrigel matrix in presence of 50 % of the conditioned media from MC3T3 cells treated with Mn or Co-substituted β-TCP and 50 % of Vascular Cell Basal Medium, maintained in culture at 37 °C in a humidified 95 %air/5 %CO_2 atmosphere for 6 hrs. The images were captured with Nikon Eclipse Ti microscope (Japan). Five fields were photographed randomly for each group, ImageJ software (http:/rsbweb.nih.gov.ij) was used to quantify branches number and total branching length which are representative of the angiogenic process in HUVECs.

2.3.5. Bone resorption pit assay

Bone resorption assay, carried out to observe the influence of the conditioned media on the osteoclastic activity, was performed as previously described [40], with little differences following described. Raw264.7 cells were seeded at a density of 5×10^4 cells/ml in 96-well plates on organic bone slices (Nordic Bioscience A/S). Bone slices originated from femoral cortical bone from cows and had a diameter of approximately 6 mm and a thickness of 0.2 mm. Raw264.7 cells seeded on bone slices were cultured in standard osteoclastic medium (OM) containing 25 ng/ml hrRANKL (positive control), in basal medium (BM) without hrRANKL (negative control) or in a mixture containing hrRANKL and conditioned medium (50 % osteoclastic medium / 50 % conditioned medium from MC3T3 treated with Mn or Co-substituted β-TCP).

The dentine discs, after 6 days of culture, were rinsed with 70 % sodium hypochlorite for 5 min and fixed in 4 % glutaraldehyde for 3 min. The resorption pits were stained using 1 % toluidine blue and observed with a light microscope (Leica DM2500 Microsystems, Germany) at a 10x magnification. Three fields of each dentin disc for each experimental point were scored in three independent experiments. The number of the pits was calculated by NIH imageJ software analysis; the results are expressed as the mean of dentine resorption pits number of eight observed fields.

2.3.6. Statistical analysis

Statistical analysis was performed with GraphPad Prism software 9.5.1. Data are reported as mean ± standard deviations (SD) at a significance level of $p < 0.05$. After having verified normal distribution and homogeneity of variance, a two-way ANOVA was done followed by Dunnett's test to detect the significant differences among materials and β-TCP at each timepoint, while Holm-Sidak's test was performed to detect the significant differences among experimental times for the same material.

3. Results and discussion

3.1. Materials synthesis and characterization

The reaction between $CaCO_3$ and $CaHPO_4 2\ H_2O$ at 1000°C yields β-TCP as unique crystalline phase, as results from the powder XRD pattern reported in Fig. 1. The analysis of the XRD patterns of the products synthesized in the presence of increasing amounts of Co^{2+} and Mn^{2+} (Fig. 1) reveals that the presence of the foreign ions allows to get β-TCP as a single crystalline phase just in limited ranges of composition. The patterns of the products synthesized in the presence of cobalt ion show the presence of a unique crystalline phase up to a Co^{2+} content of 15 at%, whereas the maximum Mn^{2+} content which yields a sole crystalline phase is 20 at%. These results are in good agreement with literature data [38, 41–44], in particular the limits are close to those reported by Nord [44] with minor variation due to the different experimental procedures. In both cases, the XRD patterns show a shift of the peaks towards higher angles as the foreign ion content increases, as clearly shown in the insets of Fig. 1. This is in agreement with a reduction of the unit cell due to the substitution of calcium (ionic radius 0.100 nm) with smaller ions (Co: 0.075 nm; Mn: 0.083 nm. The values of the lattice constants reported in Table S2 indeed confirm a significant reduction of the lattice constants on increasing Co^{2+} and Mn^{2+} contents.

Moreover, the plots of the lattice parameters reported in Fig. 2 allow to appreciate a further interesting detail of the lattice constants of Co-substituted βTCP: at variance with the variation of the *a*-axis dimension, which decreases almost linearly up to 15 at%, the variation of *c*-axis dimension shows a reversal at about 10 at%, so that its value at 15 at% is significantly higher. A similar behavior was previously observed for the substitution of magnesium ion into βTCP structure [45, 46]. The discontinuity in the c-axis variation as a function of magnesium content was found to coincide with Mg full occupancy of M(V) site and the beginning of occupancy of M(IV) site [45]. The substitution of about 10 at% is a peculiar one also in the case of Mn^{2+}, which exhibits a discontinuity in the variation of the c-axis dimension, as shown in Fig. 2.

Scanning electron microscopy images of the samples synthesized in absence of foreign ions show the characteristic morphology of β-TCP synthesized at high temperature: aggregates of micrometric particles are characterized by rounded edges (Figure S1). The increasing presence of Co provokes further aggregation of the particles, most of which appear melted together. The tendency to aggregation and melting is even more evident in the materials synthesized in the presence of Mn, which causes also a sharpening of the crystal edges. A similar behavior was previously reported for ion-substituted calcium phosphate crystals [38].

3.1.1. Structural analysis

Detailed structural features were scouted by XRD profile fittings of

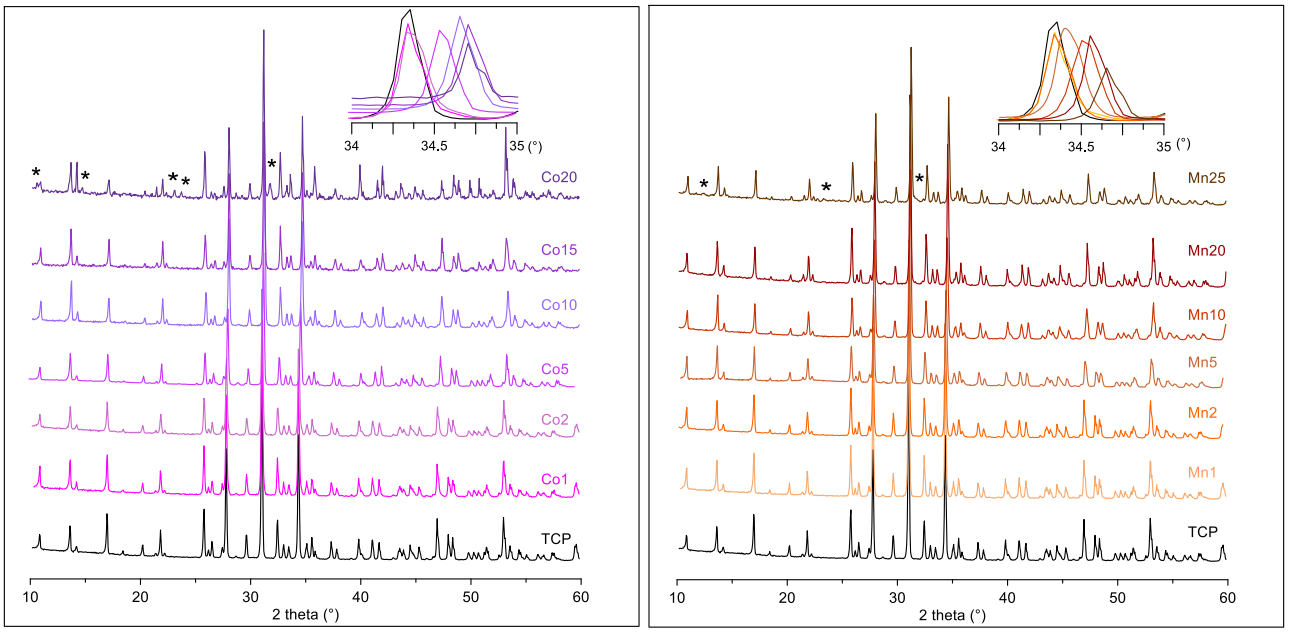

Fig. 1. XRD patterns of samples with increasing cobalt and manganese content. Asterisks highlight peaks not belonging to β-TCP crystal phase. The inset highlights the shift of the 2 2 0 peak.

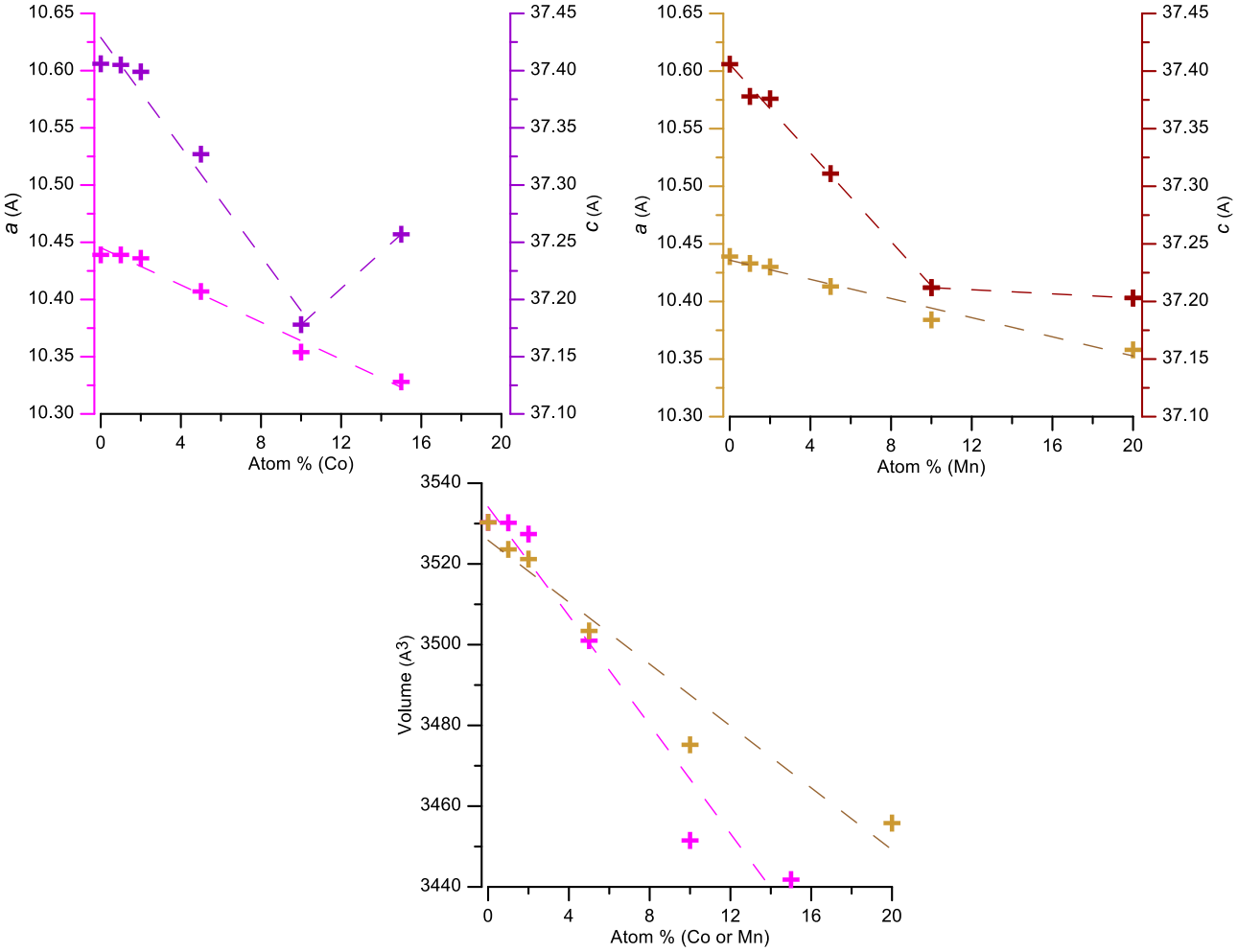

Fig. 2. Plots of the cell parameters of Co/Mn-substituted β-TCP.

samples Co5, Co15, Mn5 and Mn20, with Rietveld method. The rhombohedral β-TCP structure, reported by Dickens *et al.* [47], was used as starting model. Cobalt or manganese atoms were added as calcium substitutes in the same positions, with the following constraint of the occupation factors (OF): $OF_{Ca} + OF_{M} = 1$ for sites I, II, III, V and $OF_{Ca} + OF_{M} = 0.5$ for site IV (M = Co or Mn respectively). Because of the correlation between OF and thermal parameters, OF were fixed at the values reported in the literature [47] but an overall thermal parameter was used as variable. No constraint was imposed on the overall cobalt or manganese content, which in the final cycles resulted slightly higher than the amounts utilized in the syntheses. However, the values of content are within 3 times e.s.d. for Co15 and Mn20 samples. The higher discrepancies observed in samples at low cobalt/manganese content can be ascribed to the small difference between the scattering powers of these metals and that of calcium: the application of Rietveld method in these conditions can be considered an extreme case. The distribution of metals over the five sites is reported in Table 1.

All the samples show that the substituting ion strongly prefers site M (V), due to the shorter and more homogeneous metal-oxygen distances, which together with hexagonal coordination, make this site more suitable than the other ones for the small Co^{2+} and Mn^{2+} ions. In agreement with the lattice constants variations (Fig. 2), the variation of the M-O bond distances for the different samples reported in Fig. 3 shows that Mn substitution causes a smaller reduction than Co, in agreement with its larger ionic radius.

In the samples with the highest concentration of cobalt and manganese, Co15 and Mn20, the foreign ions are distributed also in sites M (III) and M(IV), but their presence remains scarcely appreciable in sites M(I) and M(II). The comparison of the results with the literature data of β -TCP substituted with other cations smaller than calcium, reveals that the behavior of cobalt and manganese at low concentration is more similar to that of zinc, which at low substitution rates substitutes at site M(V) [48,49], than to that of magnesium, which spreads over sites M (IV) and M(V) [45]. On the other hand, at relatively high concentration site (V) is completely filled both in cobalt and in manganese, as it has been reported for Mg [45]. The substitution with manganese reaches values higher than for cobalt and magnesium, likely because of the contribution of filling site III. The final Rietveld plots reported in Fig. 4 and **S2** confirm an overall good agreement and the absence of any secondary crystal phase.

3.2. Cellular tests

3.2.1. Cell viability and gene expression analysis

In vitro tests were carried out on disk-shaped samples of β-TCP - considered as reference material - and β-TCP partially modified by the presence of Co or Mn ions at concentrations ranging from 1 to 5 at%. Biological tests were limited to relatively low concentration of foreign ions based on the results reported in the literature on similar materials [29–33]. SEM investigation shows that the surfaces of the disk-shaped samples do not exhibit relevant morphological differences (Figure S3).

The materials were analyzed as 2 distinct groups (Co and Mn samples). The different calcium phosphates are designed for the regeneration or replacement of bone tissue [14], and the performed biological assays were primarily aimed to evaluate the ability of these materials to stimulate the osteoblasts activity. The presence of Co in bioceramic scaffolds was previously reported to stimulate angiogenesis *in vitro*, while the addition of Mn was found useful for inhibiting the activity of osteoclasts, whereas both ions promote bone regeneration [29,31,32].

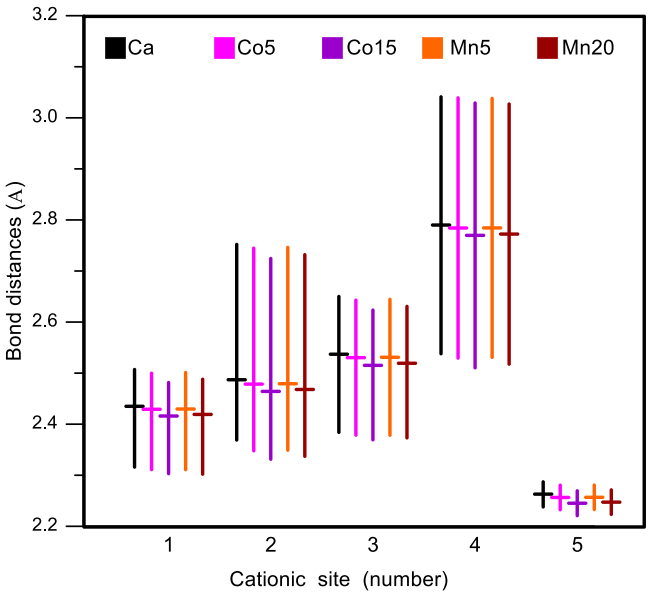

Fig. 3. Mean bond distances (horizontal bar) and distribution range of the M-O distances (vertical bar) in the different metal sites.

Herein, at first it was evaluated the viability of osteoblasts seeded on the samples. Alamar blue test highlighted a different behavior among the groups of materials: Mn samples showed a significant increase over time, except Mn5, which after 14 days showed just a weak decrease (Figure S4a), whereas Co samples showed an increase at 7 days followed by a relevant decrease at 14 days (Figure S4b). β-TCP always showed the highest levels of cell viability and a natural decrease over time due to the hyper-confluence, thus suggesting that the difference of behavior emerging by functionalized materials are ascribable to the presence of Mn or Co. These results agree with the findings of Torres, which observed a regular increase of MC3T3 viability when cultured in presence of Mn-doped β-TCP powders until 14 days of culture [35]. Using SaOS-2 treated with Co^{2+} and Cr^{3+} ions, Andrews reported a decrease in cell viability at a concentration above 100 μM [50]. Similarly, Fleury *et al.* observed analogous effects on MG-63 when cultured with Co^{2+} and Cr^{3+} ions [51]. One of the most common mechanisms underlying cytotoxicity is oxidative stress, mediated by an excess of reactive oxygen species (ROS). Cobalt has been proven to induce an oxidized state of proteins in osteoblasts, in a concentration-dependent manner, thus decreasing cell number and viability. Oxidative stress stimulates cellular

Table 1
Occupation factors and cation content from Rietveld refinements. (e.s.d. in parentheses).

Site	Multiplicity	Co5 O.F.	Co15 O.F.	Mn5 O.F.	Mn20 O.F.	Mean Ca-O§
M(I)	18	0	0	0	0.070(5)	2.44 8
M(II)	18	0	0.043(7)	0	0.054(5)	2.49 8
M(III)	18	0	0.102(7)	0	0.246(5)	2.54 8
M(IV)	6	0.08(1)	0.20(1)	0.07(1)	0.195(8)	2.79 6
M(V)	6	0.693(5)	1.000(8)	.624(4)	0.950(7)	2.26 6
Co or Mn	in unit cell	4.6(1)	9.8(4)	4.16(8)	13.5(4)	
Co or Mn	atom %*	7.3(2)	15.6(6)	6.6(1)	21.3(6)	
R_{wp}		3.4	2.7	4.8	5.1	

* Calculated on the overall cations
§ Mean Ca-O distance in β -TCP and coordination number [47]

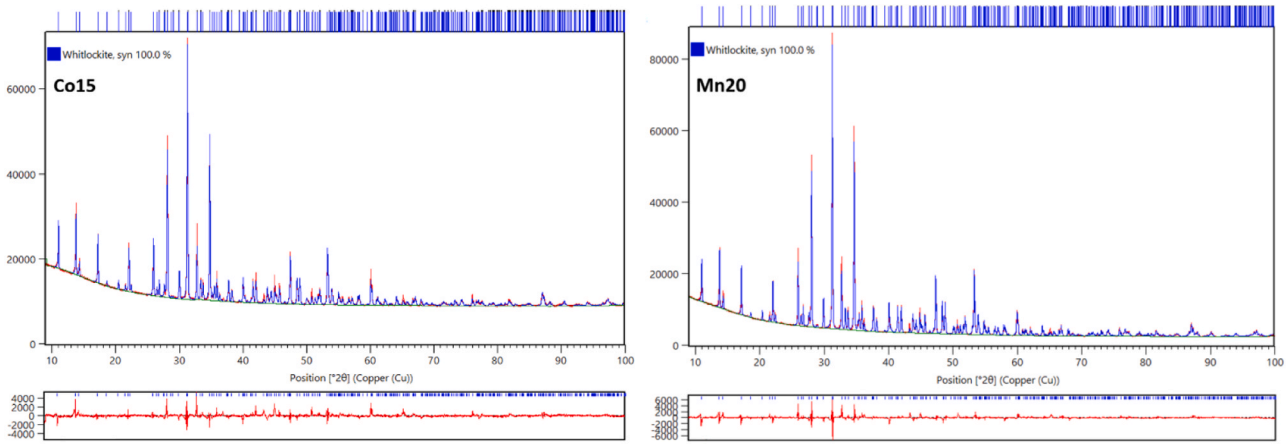

Fig. 4. Comparison of the observed (blue) and calculated (red) patterns of Co15 and Mn20. At the bottom reflection markers and difference curve are displayed.

defenses in term of antioxidant enzymes such as catalase, glutathione peroxidase, and heme oxygenase-1: the presence of the cobalt ion tends to induce the expression of these enzymes in a dose-dependent manner. Overall, however, this response is not sufficient to balance the negative effects of the oxidized state [51]. Conversely, Mn ion is known to be cofactor of antioxidant enzymes, for instance superoxide dismutase, and it plays a pivotal role in inhibiting oxidative stress [52]. This aspect is certainly crucial to understanding the divergent results between Co and Mn obtained in the cell viability assay.

Our model, based on the direct contact between cells and the solid materials, probably makes even more pronounced the differences among the materials in comparison with what observed in other models described in literature, often based on the use of extracts or powders.

In order to better understand the role of the β-TCP modifications on osteoblasts activity, the expression of some key genes was investigated. RUNX family transcription factor 2 (*Runx2*) is known to enhance the proliferation of osteoblast progenitors and regulate the expression of some bone protein genes, including alkaline phosphatase (*Alpl*), Collagen I (*Col1a1*) and bone gamma carboxyglutamate protein (*Bglap*), also named osteocalcin [53–55]. All Mn samples showed increasing levels of *Runx2* over time, even if with different timing and not always significantly, while Co1 and Co5 reached values significantly higher than β-TCP at 2 weeks (Fig. 5**a**).

The expression of *Alpl* (gene encoding for the enzyme that catalyze the hydrolysis of phosphomonoesters into inorganic phosphates, crucial for bone maturation) partially reflected what observed about *Runx2*: the values of Mn1 and Mn5 were significantly higher than β-TCP already after 24 hrs of culture, confirming this behavior after 14 days (Fig. 5**b**). *Col1a1* (gene encoding for the most abundant protein in bone matrix) showed a regular upward trend over time, reaching values much higher than β-TCP at 14 days, especially from the most Mn-rich material (Fig. 5**c**). The early phase of preosteoblast differentiation seemed thus completed in 2 weeks. Consistently, *Bglap* (gene encoding a protein required for the alignment of apatite crystals parallel to collagen fibers) being a late marker of differentiation, showed an increase on Mn1 after 7 days and a more pronounced increase on Mn5 after 14 days (Fig. 5**d**), thus confirming the relevant osteogenic stimulus provided by the highest Mn content. [25,52,54].

Runx2 expressed by osteoblasts seeded on Co-substituted β-TCP showed a less regular trend than the Mn group and, although it increased at 2 weeks, always showed lower values than the reference material (Fig. 5**e**). The expression of *Alpl* (Fig. 5**f**) was partially similar to what observed for *Runx2*: a decrease after 7 days, followed by recovery after a further 7 days. Only Co1, however, exceeded the β-TCP value at 2 weeks. Interestingly, *Col1a1* (Fig. 5**g**) moved as *Alpl* and *Runx2* regarding to fluctuations over time, but after 2 weeks of culture all Co-substituted β-TCP showed significantly higher values than β-TCP, and Co5 enhanced more strongly the expression of *Col1a1* than *Alpl*. The expression of *Bglap,* on the other hand, was always close to zero (Fig. 5**h**). The whole data of molecular biology inherent the Co group suggests that this β-TCP modification provides only a slight improvement in terms of osteogenesis. Similarly to what observed for viability assay, also the osteoblast activity seemed differently influenced by the two ions. Oxidative stress plays a role in inhibiting osteoblast activity, while superoxide dismutase, by neutralizing ROS formation, is useful in restoring regular activity of this cell type, such as mineralization. Also in this case Mn shows an essential biological role as part of antioxidant enzymes and thus as osteogenesis enhancer [52]. Li J. et al. demonstrated also the involvement of Mn-bioceramics in scavenging ROS through activation of the Nrf2 signaling pathway [32].

To extend the investigations to other functions of Mn and Co, the expression of vascular endothelial growth factor (*VEGFA*) was observed. This gene was significantly more expressed by Mn2 and Mn5 than β-TCP after 14 days, as result of a regular increase over time (Fig. 6**a**). Even more interesting, Co samples showed an expression of *VEGFA* much higher than β-TCP: at 7 days Co1 and Co2 showed a significant increase on comparison to the previous timepoint, with values higher than β-TCP, further exceeded by Co5 at 14d (Fig. 6**b**).

3.2.2. *Tube formation assay*

An *in vitro* tube formation assay was performed to evaluate the angiogenic properties of the supernatant derived from direct contact of Mn (1, 2, 5) and Co (1, 2, 5) substituted β-TCP with MC3T3-E1 pre-osteoblast after 1, 7 and 14 days (Figure S5).

The quantitative analysis of the number of branches and the total length of the branches, as shown in Fig. 6 **(c-f)**, revealed that overall the HUVECs cells were stimulated by the presence of Mn or Co.

All supernatants of Mn samples collected from MC3T3 cultures after 14 days had a significant effect on the angiogenic behavior of HUVEC cells when exposed to the supernatants for 6 hrs, as shown in Fig. 6 **(c,e)**. This finding is supported by the literature, which highlights the influence of transition metal elements, such as Mn, Fe and Co, on important biological functions, such as osteogenesis and angiogenesis [56,57]. In particular, Han J et al. clarified the mechanism of action of manganese, as Mn has a significant modulatory effect on the HIF-1 signaling pathway, reducing HIF-1α degradation, thus increasing its intracellular levels, through inhibition of HIF-prolyl hydroxylase, resulting in increased VEGF production [58]. Likely, this accounts for the increased VEGF production in MC3T3, from which the conditioned medium used to treat HUVEC cells in the tube formation assay is derived, and their rearrangement to form tubules.

Similar pro-angiogenic behavior is also observed with Co-substituted β-TCP, as shown in Fig. 6 **(d,f)**. At variance with the effects of Mn supernatants, however, the most significant results were obtained when

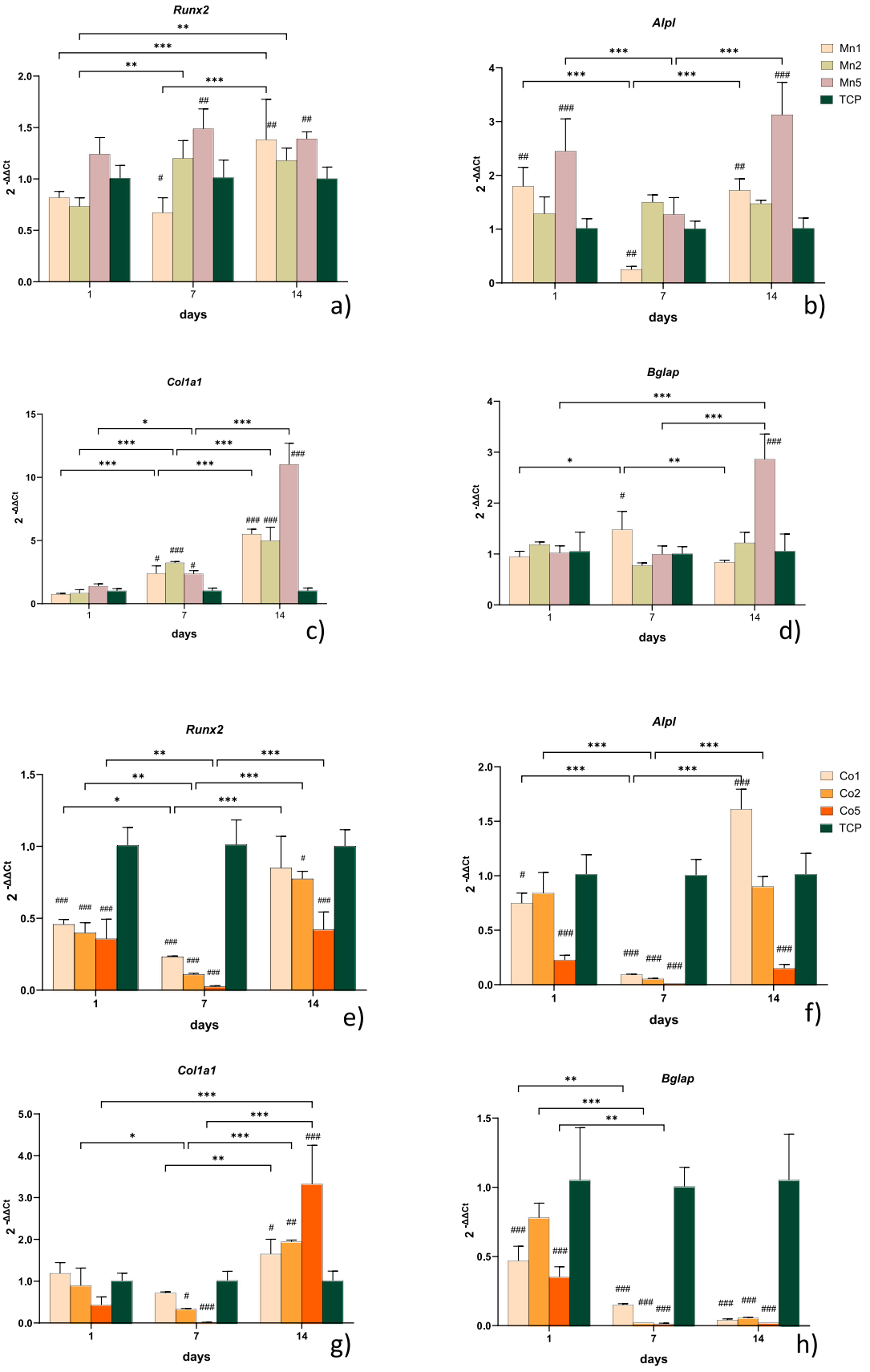

Fig. 5. Gene expression of common markers of osteoblast differentiation *Runx2, Alpl, Col1a1, Bglap* after 1, 7 and 14 days of MC3-T3 culture on β-TCP-Mn substituted (a, b, c, d) and Co-substituted (e, f, g, h). (Mean ± SD, 4 replicates). The results are normalized to *Gapdh* and expressed as fold change relative to the reference group (β-TCP) considered as 1. Statistical analysis is reported in the graphs. Dunnet's test ($^{\#}$, $p<0.05$, $^{\#\#}$, $p<0.005$, $^{\#\#\#}$, $p<0.001$): each material versus control (TCP) at each timepoint. Holm-Sidaks test (*, $p<0.05$, **, $p<0.005$, ***, $p<0.001$): comparison among experimental time for the same material.

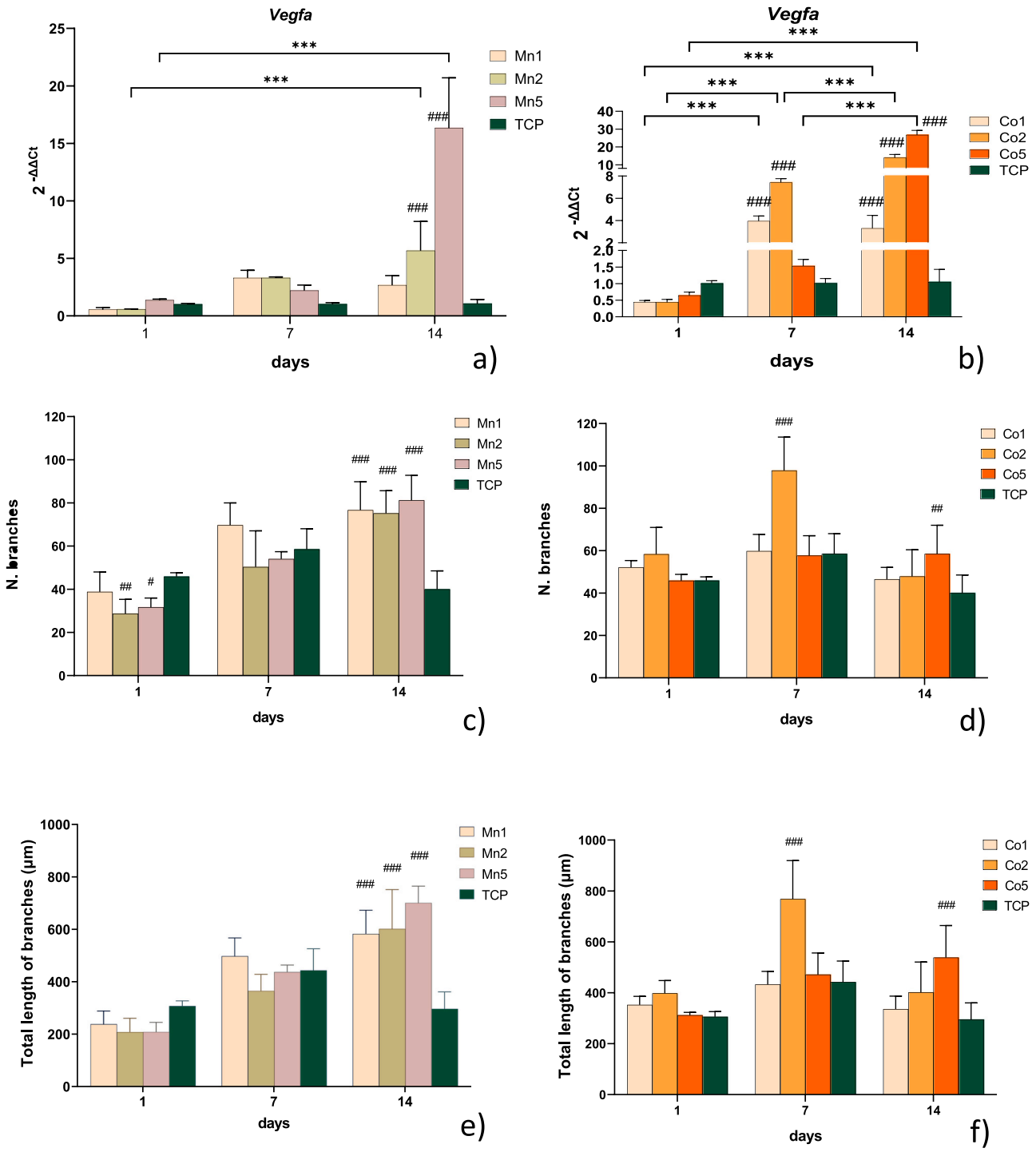

Fig. 6. In vitro angiogenic properties of materials. *Vegfa* expression after 1, 7 and 14 days of MC3T3 culture on β-TCP-Mn substituted (a) and Co-substituted (b). (Mean±SD, 4 replicates). The results are normalized to *Gapdh* and expressed as fold change relative to the reference group (β-TCP) considered as 1. Number (c, e) and total length (d, f) of branches resulting from HUVEC organization in presence of Mn or Co conditioned supernatants. The results are expressed as Mean ± SD of six observed fields. Statistical analysis is reported in the graph. Dunnet's test ($^{\#}$, $p<0.05$, $^{\#\#}$, $p<0.005$, $^{\#\#\#}$, $p<0.001$): each material versus control (TCP) at each timepoint. Holm-Sidaks test (***, $p<0.001$): comparison among experimental time for the same material.

HUVEC were treated with Co2 and Co5 supernatants. In particular, HUVEC cells showed a significant ability to sprout and self-organize into branched nodes and circles, forming continuous tubular networks, after 6 hours in culture with the supernatant from MC3T3 cells cultured with Co2 for 7 days. Instead, Co5 supernatant showed a significant effect when recovered from MC3T3 cells cultured with Co5-substituted β-TCP for 14 days.

As reported in literature, cobalt induces a hypoxia-mimicking microenvironment and positively affects the expression of *Vegfa* [59], in cells via the stabilization of hypoxia-inducible factor 1-α (HIF-1α) protein levels [60], which stimulates migration, proliferation and formation of tubular structures in HUVEC cells. This mechanism explains what is likely to happen to MC3T3 cells when they are cultured on Co-substituted β-TCP and the angiogenic effect that the conditioned media harvested from these cultures have on HUVEC cells.

3.2.3. Bone resorption activity

Bone remodeling is guaranteed by a dynamic balance regulated by bone-forming cells, osteoblasts, and bone-resorbing cells, osteoclasts; alterations in these mechanisms are responsible for a series of bone diseases.

It is interesting to evidence that Mn ions have been noticed in bone regeneration not only for their ability to sustain osteogenic differentiation, but also to inhibit osteoclastogenesis and bone resorptive functions by reducing the expression of osteoclast-specific differentiation markers [32,61,62]. In order to investigate the effects induced by Mn-substituted β-TCP on osteoclast bone resorption activity, we have exploited the ability of osteoclasts to leave "pits" after bone matrix resorption by performing Pit Assay. After co-culture of osteoclasts with the conditioned medium obtained from MC3T3 cells treated with Mn samples, the number of resorption pits was scored microscopically (Figure S6).

As shown in Fig. 7**a**, the conditioned medium from β-TCP did not have an inhibitory effect on the osteoclastic differentiation; the mature OCs have eroded dentins as evidenced by the high number of lacunae, with the highest values at 14 days. Instead, bone resorption activity was negatively affected when osteoclasts were co-cultured with the conditioned medium from Mn-substituted β-TCP. The results were similar for the different Mn concentrations, although Mn2 had the greatest inhibitory effect at all three times analyzed.

Patntirapong S. *et al.* demonstrated that the accumulation of Co in the bone mineral may have an effect on osteolysis through the increasing of both osteoclast differentiation and resorptive function. To test this, the authors delivered micromolar concentrations of Co to developing osteoclast precursors and reported that soluble Co induced directly resorption [63]. Notably, the authors reported that low doses of Co appeared to stimulate osteoclast resorptive activity, while the effects induced by higher doses needed to be better investigated. Likewise, Co-containing calcium phosphate promoted resorption of biomineralized collagen by osteoclasts [64]. In this study, we observed a reduced effect on osteoclast bone resorption activity of the conditioned medium from MC3T3 treated with Co samples, compared to β-TCP; however, when osteoclast precursors were treated with the conditioned medium from MC3T3 cultured on Co1, the number of pits increased between 1 and 7 days of culture and reached values similar to βTCP, although no significant difference was observed between these materials (Fig. 7**b**).

Looking at the above results, it is evident that all Mn-substituted-β-TCP samples, quite similarly, were able to preserve a good osteoblast viability significantly improving osteogenic and angiogenic stimuli, as well as demonstrating a role in inhibiting bone resorption by osteoclasts. At variance, in the presence of Co osteoblasts viability could be partially compromised. Nevertheless, a partial osteogenic stimulus (in terms of *Alpl* and *Col1a1* expression) was observed at the longest timepoint, angiogenic triggering was appreciable for Co2 and Co5, and osteoclast inhibition appeared preserved.

This different behavior could be related to the ionic release in cell growth medium reported in Figure S7. Mn1 and Mn2 release just a small percentage of manganese, whereas Mn release from Mn5 into the culture medium shows a "boost release" over time.

This phenomenon could be due to the peculiar characteristics of the most Mn-rich βTCP, but also to the interaction between material and cells, which could accelerate the degradation of the material and the consequent ionic release [32]. Conversely, the release of Co, which is quantitatively similar to Mn at the lowest concentration, but significantly lower from Co5 than from Mn5, elicited less effective biological responses and a decline in cell viability over time.

The above reported results suggest that modulation of Mn and Co substitution in the structure of β-TCP can be utilized to reach an excellent osteoinductivity.

4. Conclusions

The results of this work indicate that Co^{2+} and Mn^{2+} can substitute calcium in the structure of β-TCP up to a maximum amount of 15 and 20 at%, respectively. Introduction of both the foreign ions provokes a reduction of the unit cell, more evident in the case of the smaller cobalt ion. The variation of the dimensions of the lattice constants is linear for the a-axis, whereas the dimensions of the c-axis show a discontinuity at about 10 at%, as previously reported for Mg ion [45]. Detailed power pattern refinements reveal that both cobalt and manganese exhibit a clear preference for the octahedral site (V) This site is almost the only occupied one at low ionic substitution and is completely filled in Co15 and Mn20 samples.

The results of cellular tests carried out on Mn-substituted-β-TCP and Co-substituted- β-TCP at relatively low degree of substitution reveal a different influence of the two ions on cell response. Mn samples show a good osteoblast viability, significant osteogenic and angiogenic properties, and an inhibiting effect on osteoclast bone resorption. The presence of Co significantly reduces osteoblasts viability in comparison to that of β-TCP and provokes a modest osteogenic improvement. However, all Co samples inhibit osteoclast bone resorption, whereas Co2 and Co5 exhibit good angiogenic properties.

CRediT authorship contribution statement

Stefania Pagani: Writing – original draft, Validation, Methodology, Investigation, Formal analysis, Data curation. **Massimo Gazzano:** Visualization, Methodology, Investigation, Formal analysis, Data

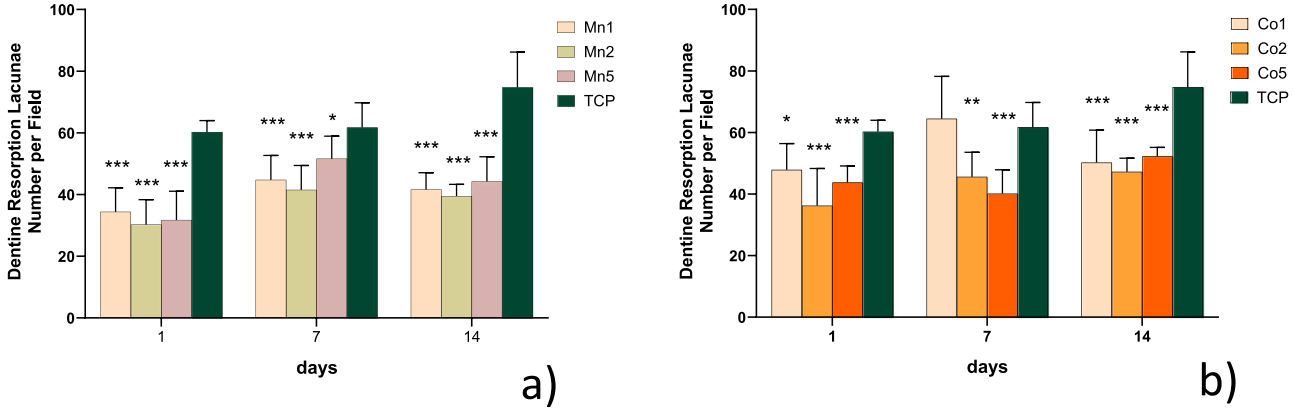

Fig. 7. Number of dentine resorption lacunae scored after 6 days of RAW 264.7 culture in presence of Mn (a) or Co (b) conditioned supernatants. The results are expressed as Mean ± SD of eight observed fields. Statistical analysis is reported in the graph. Dunnet's test (*, $p<0.05$, **, $p<0.005$, ***, $p<0.001$): each material versus control (β-TCP) at each timepoint.

curation. **Elisa Boanini:** Writing – review & editing, Writing – original draft, Visualization, Supervision, Resources, Methodology, Investigation, Data curation, Conceptualization. **Angela De Luca:** Visualization, Investigation, Formal analysis. **Alessia Romanelli:** Investigation, Data curation. **Katia Rubini:** Visualization, Investigation, Data curation. **Lavinia Raimondi:** Investigation, Formal analysis, Data curation. **Gianluca Giavaresi:** Supervision, Resources. **Adriana Bigi:** Writing – review & editing, Writing – original draft, Supervision, Methodology, Conceptualization.

Declaration of Competing Interest

The authors declare that they have no known competing financial interests or personal relationships that could have appeared to influence the work reported in this paper.

Data availability

Data will be made available on request.

Acknowledgments

The authors are grateful to Italian Ministry of Health: 5 ×1000 project, year 2020, "Fattori legati al paziente e ruolo del microambiente patologico nel potenziale rigenerativo/riparativo di terapie cellulari ed acellulari in medicina rigenerativa muscoloscheletrica".

Appendix A. Supporting information

Supplementary data associated with this article can be found in the online version at doi:10.1016/j.colsurfb.2024.114154.

References

[1] C. Giacovazzo, H.L. Monaco, G. Artioli, D. Viterbo, M. Milanesio, G. Gilli, P. Gilli, Giuseppe Zanotti, G. Ferraris, M. Catti, Fundamentals of Crystallography. International Union of Crystallography Texts on Crystallography, 3rd edn, Oxford Academic, 17 Dec. 2013, https://doi.org/10.1093/acprof:oso/9780199573653.001.0001.

[2] A. Bigi, A.E. Boanini, M. Gazzano, Ion substitution in biological and synthetic apatites, in: C. Aparicio, M.P. Ginebra (Eds.), in Biomineralization and Biomaterials, Foundamentals and Applications, Woodhead Publishing (Imprint Elsevier), Cambridge, UK, 2015, pp. 235–266.

[3] J.H. Shepherd, D.V. Shepherd, S.M. Best, Substituted hydroxyapatites for bone repair, J. Mater. Sci. Mater. Med. 23 (2012) 2335–2347, https://doi.org/10.1007/s10856-012-4598-2.

[4] M. Šupová, Substituted hydroxyapatites for biomedical applications: a review, Ceram. Int. 41 (2015) 9203–9231, https://doi.org/10.1016/j.ceramint.2015.03.316.

[5] A. Laskus, J. Kolmas, Ionic substitutions in non-apatitic calcium phosphates, Int. J. Mol. Sci. 18 (22 pages) (2017) 2542, https://doi.org/10.3390/ijms18122542.

[6] G. Graziani, M. Boi, M. Bianchi, A review on ionic substitutions in hydroxyapatite thin films: towards complete biomimetism, Coatings 8 (2018) 269, https://doi.org/10.3390/coatings8080269.

[7] D. Arcos, M. Vallet-Regi, Substituted hydroxyapatite coatings of bone implants, J. Mater. Chem. B 8 (2020) 1781–1800, https://doi.org/10.1039/c9tb02710f.

[8] F. Salamanna, G. Giavaresi, D. Contartese, A. Bigi, E. Boanini, A. Parrilli, R. Lolli, A. Gasbarrini, G. Barbanti Brodano, M. Fini, Effect of strontium substituted ß-TCP associated to mesenchymal stem cells from bone marrow and adipose tissue on spinal fusion in healthy and ovariectomized rat, J. Cell. Physiol. 234 (2019) 20046–20056, https://doi.org/10.1002/jcp.28601.

[9] D.N. da Rocha, L.R. de, Oliveira Cruz, J.B. de Campos, J.L. dos Santos, R.L.S. Blazutti Marçal, D.Q. Mijares, R.M. Barbosa, P.G. Coelho, M.H.P. da Silva, Bioactivity of strontium-monetite coatings for biomedical applications, Ceram. Int. 45 (2019) 7568–7579, https://doi.org/10.1016/j.ceramint.2019.01.051.

[10] J.V. Rau, I.V. Fadeeva, A.S. Fomin, K. Barbaro, E. Galvano, A.P. Ryzhov, F. Murzakhanov, M. Gafurov, S. Orlinskii, I. Antoniac, V. Uskoković, Sic Parvis Magna: manganese-substituted tricalcium phosphate and its biophysical properties, ACS Biomater. Sci. Eng. 5 (2019) 6632–6644, https://doi.org/10.1021/acsbiomaterials.9b01528.

[11] E. Boanini, S. Pagani, M. Tschon, K. Rubini, M. Fini, A. Bigi, Monetite vs. brushite: different influences on bone cell response modulated by strontium functionalization, J. Funct. Biomater. 13 (2022) 65, https://doi.org/10.3390/jfb13020065.

[12] J. Linares, A.B. Fernańdez, M.J. Feito, M.C. Matesanz, S. Sańchez-Salcedo, D. Arcos, M. Vallet-Regı, J.M. Rojo, M.T. Portoleś, Effects of nanocrystalline hydroxyapatites on macrophage polarization, J. Mater. Chem. B 4 (2016) 1951–1959, https://doi.org/10.1039/c6tb00014b.

[13] I. Kovrlija, J. Locs, D. Loca, Octacalcium phosphate: Innovative vehicle for the local biologically active substance delivery in bone regeneration, Acta Biomater. 135 (2021) 27–47, https://doi.org/10.1016/j.actbio.2021.08.021.

[14] A. Bigi, E. Boanini, Functionalized biomimetic calcium phosphates for bone tissue repair, J. Appl. Biomater. Funct. Mater. 15 (2017) e313–e325, https://doi.org/10.3390/jfb9010006.

[15] M. Bohner, B.Le. Gars Santoni, N. Döbelin, β-tricalcium phosphate for bone substitution: Synthesis and properties, Acta Biomater. 113 (2020) 23–41, https://doi.org/10.1016/j.actbio.2020.06.022.

[16] M. Yashima, A. Sakai, T. Kamiyama, A. Hoshikawa, Crystal structure analysis of β-tricalcium phosphate $Ca_3(PO_4)_2$ by neutron powder diffraction, J. Solid State Chem. 175 (2003) 272–277, https://doi.org/10.1016/S0022-4596(03)00279-2.

[17] E.E. Jay, E.M. Michie, D. Parfitt, M.J.D. Rushton, S.K. Fong, P.M. Mallinson, B. L. Metcalfe, R.W. Grimes, Predicted energies and structures of β-$Ca_3(PO_4)_2$, J. Solid State Chem. 183 (2010) 2261–2267, https://doi.org/10.1016/j.jssc.2010.08.008.

[18] K. Matsunaga, T. Kubota, K. Toyoura, A. Nakamura, First-principles calculations of divalent substitution of Ca^{2+} in tricalcium phosphates, Acta Biomater. 23 (2015) 329–337, https://doi.org/10.1016/j.actbio.2015.05.014.

[19] G.A. Sblendorio, B. Le Gars Santoni, D.T.L. Alexander, P. Bowen, M. Bohner, N. Döbelin, Towards an improved understanding of the β-TCP crystal structure by means of "checkerboard" atomistic simulations, J. Eur. Ceram. Soc. 43 (2023) 3746–3754, https://doi.org/10.1016/j.jeurceramsoc.2023.02.036.

[20] E. Boanini, M. Gazzano, C. Nervi, M.R. Chierotti, K. Rubini, R. Gobetto, A. Bigi, Strontium and zinc substitution in β-tricalcium phosphate: an X-ray diffraction, solid state NMR and ATR-FTIR study, J. Funct. Biomater. 10 (2019) 20, https://doi.org/10.3390/jfb10020020.

[21] H. Cummings, W. Han, S. Vahabzadeh, S.F. Elsawa, Cobalt-doped brushite cement: preparation, characterization, and in vitro interaction with osteosarcoma cells, Jom 69 (2017) 1348–1353, https://doi.org/10.1007/s11837-017-2376-9.

[22] T. Tian, Y. Han, B. Ma, C. Wu, J. Chang, Novel Co-akermanite ($Ca_2CoSi_2O_7$) bioceramics with the activity to stimulate osteogenesis and angiogenesis, J. Mater. Chem. B 3 (2015) 6773–6782, https://doi.org/10.1039/C5TB01244A.

[23] J. Zhou, L. Zhao, Hypoxia-mimicking Co doped TiO_2 microporous coating on titanium with enhanced angiogenic and osteogenic activities, Acta Biomater. 43 (2016) 358–368, https://doi.org/10.1016/j.actbio.2016.07.045.

[24] N. Ignjatović, Z. Ajduković, J. Rajković, S. Najman, D. Mihailović, D. Uskoković, Enhanced osteogenesis of nanosized cobalt-substituted hydroxyapatite, J. Bionic Eng. 12 (2015) 604–612, https://doi.org/10.1016/S1672-6529(14)60150-5.

[25] T. Wu, H. Shi, Y. Liang, T. Lu, Z. Lin, J. Ye, Improving osteogenesis of calcium phosphate bone cement by incorporating with manganese doped β-tricalcium phosphate, Mater. Sci. Eng. C. 109 (2020) 110481, https://doi.org/10.1016/j.msec.2019.110481.

[26] A. Bernhardt, M. Schamel, U. Gbureck, M. Gelinsky, Osteoclastic differentiation and resorption is modulated by bioactive metal ions Co^{2+}, Cu^{2+} and Cr^{3+} incorporated into calcium phosphate bone cements, 12e0182109, PLoS ONE (2017), https://doi.org/10.1371/journal.pone.0182109.

[27] Z. Chen, J. Yuen, R. Crawford, J. Chang, C. Wu, Y. Xiao, The effect of osteoimmunomodulation on the osteogenic effects of cobalt incorporated b-tricalcium phosphate, Biomaterials 61 (2015) 126–138, https://doi.org/10.1016/j.biomaterials.2015.04.044.

[28] B. Bracci, P. Torricelli, S. Panzavolta, E. Boanini, R. Giardino, A. Bigi, Effect of Mg^{2+}, Sr^{2+}, and Mn^{2+} on the chemico-physical and in vitro biological properties of calcium phosphate biomimetic coatings, J. Inorg. Biochem. 103 (2009) 1666–1674, https://doi.org/10.1016/j.jinorgbio.2009.09.009.

[29] J. Li, C. Zhao, C. Liu, Z. Wang, Z. Ling, B. Lin, Bi Tan, L. Zhou, Y. Chen, D. Liu, X. Zou, W. Liu, Cobalt-doped bioceramic scaffolds fabricated by 3D printing show enhanced osteogenic and angiogenic properties for bone repair, BioMed. Eng. OnLine 20 (2021) 70, https://doi.org/10.1186/s12938-021-00907-2.

[30] P.M.C. Torres, A. Marote, A.R. Cerqueira, A.J. Calado, J.C.C. Abrantes, S.Olhero S, O.A.B. da Cruz e Silva, S.I. Vieira, J.M.F. Ferreira, Injectable MnSr-doped brushite bone cements with improved biological performance, J. Mater. Chem. B 5 (2017) 2775–2787, https://doi.org/10.1039/C6TB03119F.

[31] F. Silingardi, F. Salamanna, M. Español, M. Maglio, M. Sartori, G. Giavaresi, A. Bigi, M.P. Ginebra, E. Boanini, Regulation of osteogenesis and angiogenesis by cobalt, manganese and strontium doped apatitic materials for functional bone tissue regeneration, ISSN 2772-9508, Biomater. Adv. (2024) 213968, https://doi.org/10.1016/j.bioadv.2024.213968.

[32] J. Li, C. Deng, W. Liang, F. Kang, Y. Bai, B. Ma, C. Wu, S. Dong, Mn-containing bioceramics inhibit osteoclastogenesis and promote osteoporotic bone regeneration via scavenging ROS, Bioact. Mater. 6 (2021) 3839–3850, https://doi.org/10.1016/j.bioactmat.2021.03.039.

[33] M. Zhang, C. Wu, H. Li, J. Yuen, J. Chang, Y. Xiao, Preparation, characterization and in vitro angiogenic capacity of cobalt substituted β-tricalcium phosphate ceramics, J. Mater. Chem. 22 (2012) 21686–21694, https://doi.org/10.1039/C2JM34395A.

[34] Y. Zheng, Y. Yang, Y. Deng, Dual therapeutic cobalt-incorporated bioceramics accelerate bone tissue regeneration, Mater. Sci. Eng.: C. 99 (2019) 770–782, https://doi.org/10.1016/j.msec.2019.02.020.

[35] P.M.C. Torres, S.I. Vieira, A.R. Cerqueira, S. Pina, O.A.B. da Cruz Silva, J.C. C. Abrantes, J.M.F. Ferreira, Effects of Mn-doping on the structure and biological properties of β-tricalcium phosphate, J. Inorg. Biochem. 136 (2014) 57–66, https://doi.org/10.1016/j.jinorgbio.2014.03.013.

[36] G. Cheng, C. Deng, C. Wu, H. Yin, Y. Ruan, Y. Sun, Q. Xie, X. Wu, Effects of Mn-doping on the structural evolution of β-Tricalcium phosphate by Rietveld

refinement and Raman spectroscopy, Mater. Lett. 235 (2019) 236–238, https://doi.org/10.1016/j.matlet.2018.10.031.
[37] J. Che, H. Wang, Y. Ma, F. Cao, G. Liu, W. Shang, X. Lv, T. Sun, J. Tong, Effects of Mn-doping on the structure and in vitro degradation of β-tricalcium phosphate, Ceram. Int. 47 (2021) 22994–23000, https://doi.org/10.1016/j.ceramint.2021.05.013.
[38] A. Altomare, R. Rizzi, M. Rossi, A. El Khouri, M. Elaatmani, V. Paterlini, G. Della Ventura, F. Capitelli, New $Ca_{2.90}(Me^{2+})_{0.10}(PO_4)_2$ β-tricalcium phosphates with Me^{2+} = Mn, Ni, Cu: Synthesis, crystal-chemistry, and luminescence properties, Crystals 9 (2019) 288, https://doi.org/10.3390/cryst9060288.
[39] T.D. Schmittgen, K.J. Livak, Analyzing real-time PCR data by the comparative C(T) method, Nat. Protoc. 3 (2008) 1101–1108, https://doi.org/10.1038/nprot.2008.73.
[40] L. Raimondi, A. De Luca, S. Fontana, N. Amodio, V. Costa, V. Carina, D. Bellavia, S. Raimondo, S. Siragusa, F. Monteleone, R. Alessandro, M. Fini, G. Giavaresi, Multiple myeloma-derived extracellular vesicles induce osteoclastogenesis through the activation of the XBP1/IRE1α axis, Cancers (Basel) 12 (2020) 2167, https://doi.org/10.3390/cancers12082167.
[41] S.S. Romdhane, A. Legrouri, J. Lenzi, G. Bonel, M. Lenzi, Préparation et étude physicochimique d'orthophosphates mixtes, Rev. Chim. Miner. 21 (1984) 299.
[42] A. Legrouri, S.S. Romdhane, J. Lenzi, M. Lenzi, G. Bonel, Influence of preparation method on catalytic properties of mixed calcium-cobalt orthophosphates, J. Mater. Sci. 31 (1996) 2469–2473, https://doi.org/10.1007/BF01152963.
[43] D.V. Deyneko, V.N. Lebedev, K. Barbaro, V.V. Titkov, B.I. Lazoryak, I.V. Fadeeva, A.N. Gosteva, I.L. Udyanskaya, S.M. Aksenov, J.V. Rau, Antimicrobial and cell-friendly properties of cobalt and nickel-doped tricalcium phosphate ceramics, Biomimetics 9 (2024) 14, https://doi.org/10.3390/ biomimetics9010014.
[44] A.G. Nord, Incorporation of divalent metals in whitlockite-related β-$Ca_3(PO_4)_2$, Neue Jahrb. Miner. Mon. 11 (1983) 489–497.
[45] A. Bigi, G. Falini, E. Foresti, A. Ripamonti, M. Gazzano, N. Roveri, Rietveld structure refinement of synthetic magnesium substituted β-tricalcium phosphate, Z. Krist. 211 (1996) 13–16, https://doi.org/10.1524/zkri.1996.211.1.13.
[46] S. Kannan, F. Goetz-Neunhoeffer, J. Neubauer, S. Pina, P.M.C. Torres, J.M. F. Ferreira, Synthesis and structural characterization of strontium- and magnesium-co-substituted β-tricalcium phosphate, Acta Biomater. 6 (2010) 571–576, https://doi.org/10.1016/j.actbio.2009.08.009.
[47] B. Dickens, L.W. Schroeder, W.E. Brown, Crystallographic studies of the role of Mg as a stabilizing impurity in β-$Ca_3(PO_4)_2$. I. The crystal structure of pure β-$Ca_3(PO_4)_2$, J. Solid State Chem. 10 (1974) 232–248, https://doi.org/10.1016/0022-4596(74)90030-9.
[48] K. Kawabata, T. Yamamoto, A. Kitada, Substitution mechanism of Zn ions in β-tricalcium phosphate, Phys. B: Condens. Matter 406 (2011) 890–894, https://doi.org/10.1016/j.physb.2010.12.022.
[49] S. Kannan, F. Goetz-Neunhoeffer, J. Neubauer, J.M.F. Ferreira, Synthesis and structure refinement of zinc-doped β-tricalcium phosphate powders, J. Am. Ceram. Soc. 92 (2009) 1592–1595, https://doi.org/10.1111/j.1551-2916.2009.03093.x.
[50] R.E. Andrews, K.M. Shah, J.M. Wilkinson, A. Gartland, Effects of cobalt and chromium ions at clinically equivalent concentrations after metal-on-metal hip replacement on human osteoblasts and osteoclasts: Implications for skeletal health, Bone 49 (2011) 717–723, https://doi.org/10.1016/j.bone.2011.06.007.
[51] C. Fleury, A. Petit, F. Mwale, J. Antoniou, D.J. Zukor, M. Tabriziam, O.L. Huk, Effect of cobalt and chromium ions on human MG-63 osteoblasts in vitro: Morphology, cytotoxicity, and oxidative stress, Biomaterials 27 (2006) 3351–3360, https://doi.org/10.1016/j.biomaterials.2006.01.035.
[52] S. Bose, G. Fielding, S. Tarafder, A. Bandyopadhyay, Trace element doping in calcium phosphate ceramics to understand osteogenesis and angiogenesis, Trends Biotechnol 31 (2013) 594–605, https://doi.org/10.1016/j.tibtech.2013.06.005.
[53] J.H. Jonason, G. Xiao, M. Zhang, L. Xing, D. Chen, Post-translational regulation of Runx2 in bone and cartilage, J. Dent. Res 88 (2009) 693–703, doi.org/10.1177/0022034509341629.
[54] T. Komori, Whole Aspect of Runx2 Functions in Skeletal Development, Int. J. Mol. Sci. 23 (2022) 5776, https://doi.org/10.3390/ijms23105776.
[55] X. Qin, Q. Jiang, H. Komori, C. Sakane, R. Fukuyama, Y. Matsuo, K. Ito, T. Miyazaki, T. Komori, Runt-related transcription factor-2 (Runx2) is required for bone matrix protein gene expression in committed osteoblasts in mice, J. Bone Miner. Res. 36 (2021) 2081–2095, https://doi.org/10.1002/jbmr.4386.
[56] K. Meenakshi, K.R. Uday, S.G. Pravin, K.P. Nandha, N.R. Subha, Modulation of 3D printed calcium-deficient apatite constructs with varying Mn concentrations for osteochondral regeneration via endochondral differentiation, ACS Appl. Mater. Interf. 14 (2022) 23245–23259, https://doi.org/10.1021/acsami.2c05110.
[57] Z. Dongdong, L. Mei, X. Ru, X. Juning, Z. Yu, Q. Shi, Q. Yuqin, P. Feng, L. Xuanyong, Complementary and Synergistic Design of Bi-Layered Double Hydroxides Modified Magnesium Alloy toward Multifunctional Orthopedic Implants, Adv. Healthc. Mater. 12 (2023) e2201367, https://doi.org/10.1002/adhm.202201367.
[58] J. Han, J.S. Lee, D. Choi, Y. Lee, S. Hong, J. Choi, S. Han, Y. Ko, J.A. Kim, Y.M. Kim, Y. Jung, Manganese (II) induces chemical hypoxia by inhibiting HIF-prolyl hydroxylase: implication in manganese-induced pulmonary inflammation, Toxicol. Appl. Pharmacol. 235 (2009) 261–267, https://doi.org/10.1016/j.taap.2009.01.003. PMID: 19263519.
[59] L. Haiping, Z. Yinghong, M. Yaping, X. Lan, J. Wenjun, Z. Yi, W. Xin, Current Application of Beta-Tricalcium Phosphate in Bone Repair and Its Mechanism to Regulate Osteogenesis, Front. Mater. 8 (2021) 698915 doi.org/10.3389/fmats.2021.698915.
[60] Z. Xin, N. Kai, Z. Yuankai, S. Keke, G. Zilong, S. Donglong, F. Lihong, Lithium and cobalt co-doped mesoporous bioactive glass nanoparticles promote osteogenesis and angiogenesis in bone regeneration, Front, Bioeng., Biotechnol. 11 (2024) 1288393, 10.3389/fbioe.2023.1288393. eCollection 2023.
[61] L. Strause, P. Saltman, J. Glowacki, The effect of deficiencies of manganese and copper on osteoinduction and on resorption of bone particles in rats, Calcif. Tissue Int. 41 (1987) 145–150, https://doi.org/10.1007/BF02563794.
[62] B. Yun-Jung, K. Mi-Hyun, Manganese supplementation improves mineral density of the spine and femur and serum osteocalcin in rats, Biol., Trace Elem., Res 124 (2008) 28–34, https://doi.org/10.1007/s12011-008-8119-6.
[63] S. Patntirapong, P. Habibovic, P.V. Hauschka, Effects of soluble cobalt and cobalt incorporated into calcium phosphate layers on osteoclast differentiation and activation, Biomaterials 30 (2009) 548–555, https://doi.org/10.1016/j.biomaterials.2008.09.062.
[64] D. de Melo Pereira, M. Schumacher, P. Habibovic, Cobalt-containing calcium phosphate induces resorption of biomineralized collagen by human osteoclasts, Biomater. Res 25 (2021) 6, https://doi.org/10.1186/s40824-021-00209-7.